Catalysis Today 181 (2012) 4–13

Contents lists available at SciVerse ScienceDirect

Catalysis Today

journal homepage: www.elsevier.com/locate/cattod

Steam reforming of ethanol over carburized alkali-doped nickel on zirconia and various supports for hydrogen production

Masato Akiyama, Yasunori Oki, Masatoshi Nagai*

Graduate School of Bio-Applications and Systems Engineering, Tokyo University of Agriculture and Technology, 2-24 Naka-cho, Koganei, Tokyo 184-8588, Japan

ARTICLE INFO

Article history:
Received 13 March 2011
Received in revised form
17 September 2011
Accepted 24 September 2011
Available online 12 December 2011

Keywords:
Additives
Carburization
Ethanol
Cesium
Hydrogen production
Steam reforming

ABSTRACT

The steam reforming of ethanol over carburized alkali-, La- and Ce-doped nickels on zirconia and various supports was studied to determine the support effects, alkali addition and carburization. The 823 K-carburized Ni/ZrO_2 and Ni/V_2O_5 catalysts exhibited higher activities than the Ni catalysts supported on CeO_2, Al_2O_3, SiO_2–Al_2O_3 and MgO and a reduced catalyst. The cesium-doped Ni/ZrO_2 promoted more hydrogen formation than the Li-, K-, La- and Ce-doped catalysts. From the XRD measurement, crystals of ZrO_2, Ni carbide and Ni metal were formed during the carburization of the Ni/ZrO_2 catalyst at 823 K. No Ni carbide was observed on the MgO, CeO_2 Al_2O_3, and V_2O_5 carburized catalysts. The $Cs_{0.2}Ni/ZrO_2$ and $Cs_{0.5}Ni_{0.5}/Zr$ exhibited no carbon deposition at 7 h. The carburized and cesium-doped Ni/ZrO_2 was more effective in decreasing the carbon deposition. From the IR study, the formed carbonated species were attributed to the formation of CO_3^- from the formed CO_2 ($CO_2 + O_2^- \rightarrow CO_3^-$). In the pulse experiment of $H_2{}^{18}O$, $Cs_{0.2}Ni/ZrO_2$ helped to facilitate the dissociation of H_2O to 2H and O and the decomposition of CH_3CHO to hydrogen and CO_2 through the CH_3CO species. The TPD after ethanol adsorption on Ni/ZrO_2 with and without Cs-doping showed that the Cs-doped Ni/ZrO_2 catalyst promoted the C–H breaking through the CH_3CO species more than the Ni/ZrO_2 catalyst.

1. Introduction

The steam reforming of ethanol (SRE) has been studied for the production of hydrogen for polymer electrolyte fuel cell (PEFC) applications and ethylene and propylene for the plastic industry. Various noble-metal-supported Co and Ni catalysts were extensively studied for the SRE to produce hydrogen. Noble metal catalysts, such as Rh/CeO_2ZrO_2 [1–3] and Ir/CeO_2 [4], have been developed. 1% $Rh/CeO_2{\cdot}ZrO_2$ at 973 K was studied and exhibited a high activity for hydrogen production and high CO_2 selectivity due to the mobile OH group migration on the CeO_2 surface [1]. Among the noble metals, the Rh catalyst exhibited a high activity for the SRE, less carbon deposition and high durability during the reaction, but Rh is a very expensive metal. Therefore, the Rh catalyst has this concern for promoting a practical process. The transition metals, such as Co and Ni, for a high C–C bond scission, are used for the C–C bond scission of ethanol rather than the C–O bond scission. The cobalt catalysts, such as Co/CeO_2 [5], Co/CeO_2ZrO_2 [6] and Co/ZnO [7], exhibited a very significant hydrogen production with less carbon deposition. The ceria-supported Ni catalyst was reported to be more active than the Co and Ir catalysts for hydrogen production and to have less CO selectivity at 723 K [8]. Regarding the Ni catalyst, it has a high activity for the C–C bond scission during the SRE. However, the Ni catalyst has a troublesome problem, such as catalyst deactivation, due to a high carbon deposition. As a result, catalysts have been developed that resist carbon deposition; i.e., Ni supported on Y_2O_3, La_2O_3 [9,10], and CeO_2 [11,12] for reducing carbon deposition, ZrO_2 with a stabilizer of Y_2O_3 for CO reduction [13], La_2O_3 [14,15] and K [16] doped γ-Al_2O_3 for the reduction of Ni, and alkali promoted Ni/MgO for depressing the Ni sintering and coke formation [17,18]. The Ni metal alloys, such as the ceria-modified $NiZn/Al_2O_3$ for decreasing coke deposition [19], $NiCuK/Al_2O_3$ [20] and NiCu/SBA-15 [21] for the formation of smaller metallic crystallite sizes, have been studied but were not relatively active for hydrogen production. Furthermore, the transition metal carbides, such as Mo_2C [23–25] and NiMo carbides [22,26] and Zr·K–CoMo carbide [27] are useful for various industrial processes due to the high dissociation of water and less carbon deposition and are prepared using the temperature-programmed carburization (TPC) of their metal oxides in a stream of methane in hydrogen. Furthermore, TPD study after $H_2{}^{18}O$ desorption showed that zirconia prevented the oxidation of β-Mo_2C and potassium promoted water dissociation [27]. In this study, we selected zirconia as a support and alkali metals as promoting additives. The previous paper suggests that zirconium and alkali additives are applicable to steam reforming of

* Corresponding author. Tel.: +81 42 3887060; fax: +81 42 3887060.
E-mail address: mnagai@cc.tuat.ac.jp (M. Nagai).

0920-5861/$ – see front matter © 2011 Elsevier B.V. All rights reserved.
doi:10.1016/j.cattod.2011.09.043

ethanol involving the C–H, C–C and C–O bond-breaking reactions as well as water-gas shift ($CO + H_2O \rightarrow CO_2 + H_2$) and methanation ($CO + 3H_2 \rightarrow CH_4 + H_2O$) reactions. Although the developed SRE is a promising process, there has been little study of the carburization and effects of Ni supported on zirconia and several oxides on the SRE mechanism. In this paper, the effects of several supports, such as ZrO_2, V_2O_5, CeO_2, MgO and Al_2O_3, on the SRE activity and the difference between the carburization and reduction of Ni/ZrO_2 were studied. The active species of the Cs-doped Ni/ZrO_2 and the SRE mechanism were discussed on the basis of the TPC, temperature-programmed reduction (TPR), the pulse of $H_2{}^{18}O$ into the SRE, the temperature-programmed desorption (TPD) after ethanol adsorption and the IR bands of ethanol and the products. Also, carbon deposits present on the post-reforming catalysts were estimated by temperature-programmed oxidation (TPO).

2. Experimental

The precursors of Ni supported on oxide supports were prepared by the impregnating of ZrO_2 (Kishida Co.) with an aqueous solution of $Ni(NO_3)_2{\cdot}6H_2O$ to become 25 wt% NiO, then oxidized at 773 K in air. The supports of V_2O_5 (Kishida Co.), Al_2O_3(JRC-ALO-2), CeO_2 (Kishida Co.), SiO_2-Al_2O_3 (JRC-SAH) and MgO (Kishida Co.) were also selected. The additives, such as Li, K, Cs, La and Ce, were added to the precursor as an aqueous solution of $LiNO_3$ (Kishida Co.), K_2CO_3 (Kishida Co.), $CsNO_3$ (Wako Co.), $LaNO_3{\cdot}6H_2O$ (Wako Co.) and $CeNO_3{\cdot}6H_2O$ (Wako Co). The precursors containing Ni and the support were mixed with an additive, dried at 293 K and calcined at 773 K for 5 h in air. The oxidized precursor (0.2 g) was packed into a fixed bed flow microreactor, oxidized at 773 K in a stream of air for 0.5 h, and then cooled to 723 K. The precursor was carburized from 723 to a final temperature of 773–873 K in a stream of 20% CH_4/H_2 at the rate of 1 K/min, maintained at this temperature for 2 h and cooled to room temperature in the stream of 20% CH_4/H_2. The oxidized precursor was exposed to a stream of He at 293 K and treated from 293 to 723 K at the rate of 1 K/min in a stream of 100% H_2 for comparison of the activity and selectivity of the carburized Ni/ZrO_2 catalysts.

The SRE was carried out in situ at temperatures of 573, 673 and 773 K, a N_2 gas flow rate of 0.9 L/h, in an aqueous solution of ethanol (C_2H_5OH:H_2O molar ratio 1:13; 20.5, w/w) at the flow rate of 12 mL/h and a catalyst charging of 0.2 g after carburization. The contact time was varied with a GHSV of 3000–97,000 h^{-1}. Additionally, bioethanol was used for comparison with the aqueous ethanol feed. The bioethanol was obtained from the Juon Co. (Hiroshima prefecture), which was made from Japanese cedar with a small amount of cypress, which was crushed, converted into glucose and fructose with gluco-amyrase and fermented with yeast. The produced bioethanol contained 72% (w/w) ethanol. The reaction products were analyzed using TCD and FID-GC with a methanizer for the reaction products during the reaction.

The N_2 physical adsorption experiment with the catalysts was performed using an Ommisorp 100CX volumetric analyzer (Beckman Coulter Co.) at 77 K. The XRD analysis was conducted using an RINT2000 (Rigaku Co.) with Cu-Kα radiation. The peaks were identified on the basis of the JCPDS card references. The surface carbons of the $Ce_{0.2}Ni_{0.8}/ZrO_2$ and Ni/ZrO_2 catalysts after the reaction were evaluated by TPO analysis using a quadruple mass spectrometer (Quastar 422, Balzers Co.). The TPO was carried out from 373 to 1023 K at the rate of 10 K/min in a stream of 10% O_2/He. The deposited carbon values of the various metal-doped Ni/ZrO_2 catalysts were measured using a gravimetric method. In order to determine how the Ni catalysts interacted with the additive during the carburization, the TPC was carried out from room temperature to 973 K at the rate of 1 K/min in a stream of 20% CH_4/H_2 (66.7 mL/min). The desorption of H_2O (m/z = 18), CO (28) and CO_2 (44) was obtained. TPR was carried out by heating from room temperature to 1023 K at the rate of 10 K/min in a 15 mL/min stream of 10% hydrogen in helium after carburization at 823 K. The carburized $CsNi/ZrO_2$ and Ni/ZrO_2 catalysts were analyzed by FTIR (Nicolet, Model 6700FT-IR, MCT detector). The diffuse reflectance spectra of the catalysts were recorded at temperatures from 293 to 573 K using the FTIR instrument with a resolution of 4 cm^{-1} for 128 scans at 293 K. The catalyst was mixed with KBr powder to a 40% dilution and placed in a cell attached to the IR compartment which was directly treated in the cell. Prior to the IR measurement of ethanol, the samples were activated by heating at 603 K in a stream of He, maintained at 603 K for 4 h and then cooled to 293 K. Furthermore, TPD was carried out in situ by heating from room temperature to 1000 K at the rate of 10 K/min in a stream of Ar at 15 mL/min after ethanol was allowed to flow (170 μmol/g-cat) over the catalyst. The produced gases of H_2O, CO, CO_2, CH_4 (m/z = 16), C_2H_4 (26), CH_3CHO (29), C_2H_6 (30) and C_2H_5OH (31) were monitored using the quadruple mass spectrometer. The intensities of these gases were calculated in order to determine the fragmentations. The CH_3CHO and C_2H_4 were selected to be m/z = 29 and 26 because the compounds had molecular ion peaks of 44 and 28 with evaluation of several fragments overlapped with CO_2, N_2 and CO, respectively. Ethanol-d was used as an isotope-labeled ethanol to determine the hydrogen behavior of the hydroxyl group of the ethanol during the SRE. In order to study the oxygen behavior of water during the SRE, an isotope-labeled molecule of 2 μL $H_2{}^{18}O$ was studied in a stream of $C_2H_5{}^{16}OH$/He at 293 K. The H_2 (m/z = 2), $H_2{}^{16}O$ (18), $H_2{}^{18}O$ (20), $C^{16}O$ (28), $C^{18}O$ (30), $C^{16}O_2$ (44), $C^{16}O^{18}O$ (46) and $C^{18}O_2$ (48) were monitored.

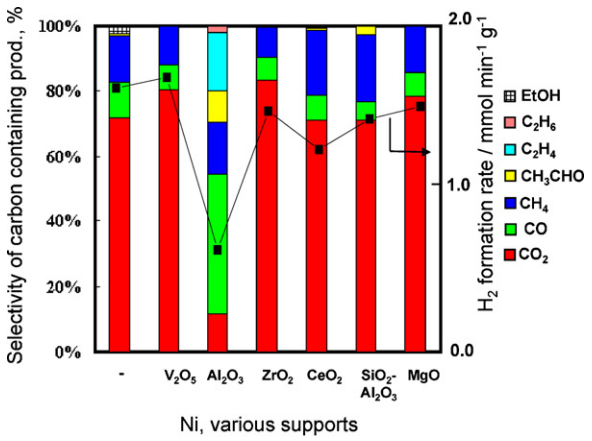

Fig. 1. The steam reforming of ethanol on the 823 K-carburized nickel on various supports at 773 K.

3. Results and discussion

3.1. Steam reforming ethanol using carburized Ni catalysts on various supports

The SRE on the 823 K-carburized 25% Ni catalysts supported on various oxides (V_2O_5, Al_2O_3, ZrO_2, CeO_2, SiO_2–Al_2O_3 and MgO) without any additives at 773 K was determined. The formation rate of hydrogen and the distribution of the reaction products are shown in Fig. 1. The carburized Ni/V_2O_5 catalyst exhibited the highest hydrogen formation rate of 1.67 mmol/min g among the catalysts. The Ni/ZrO_2 had a high hydrogen production of 1.45 mmol/min g. These catalysts were more active than the Ni/MgO, Ni/SiO_2–Al_2O_3 and Ni/CeO_2 catalysts (H_2 production, 1.2–1.48 mmol/min g) for the SRE. Ni/V_2O_5 and Ni/ZrO_2 produced CO_2 at 80% with CO and

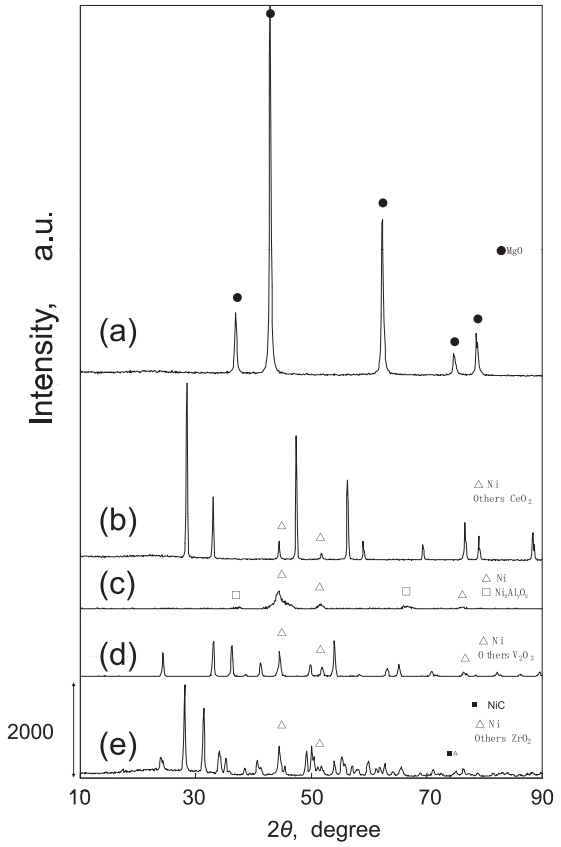

Fig. 2. The XRD patterns of carburized Ni supported on the supports of (a) MgO, (b) CeO_2, (c) Al_2O_3, (d) V_2O_5 and (e) ZrO_2.

methane at 20%. For the Ni/MgO, Ni/CeO_2 and $Ni/SiO_2{\cdot}Al_2O_3$ catalysts, CO_2 was distributed at less than 80% with 6–8% CO and methane at 10–20%. The C–H bond and C–C bond scissions of ethanol selectively occurred during the SRE. However, for the Ni/Al_2O_3 catalyst, the hydrogen formation rate was low with a high selectivity for ethylene and CO. The Ni/Al_2O_3 catalyst exhibited a large amount of CO with a high selectivity for ethylene and methane as reported in the references [28–30]. The Ni/Al_2O_3 has an acidic function and is responsible for the acidic cleavage of the CO bond of ethanol which promoted the ethylene formation.

The XRD patterns of the 25% Ni supported on MgO, CeO_2, Al_2O_3, V_2O_5, and ZrO_2 carburized at 823 K are shown in Fig. 2. Crystals of ZrO_2, Ni carbide and Ni metal were formed during the carburization of the Ni/ZrO_2 catalyst at 823 K. No Ni carbide was observed on the MgO, CeO_2 Al_2O_3, and V_2O_5 carburized catalysts. For the Ni/MgO catalyst, only MgO was observed. The Ni/Al_2O_3 catalyst contained Ni metal and nickel-alumina oxide. Furthermore, the pattern of the Ni/V_2O_5 catalyst showed that Ni metal and V_2O_3 were formed. V_2O_5 was reduced to V_2O_3 during the carburization. After the reaction, carbons were observed along with the reaction products. Furthermore, the Ni metal crystallite size was calculated from the peak at $2\theta = 44.5^\circ$ using the Scherrer equation. The Ni metal size of the carburized catalyst increased from 19.9 to 22.7 Å at 5 h after the reaction, while that of the reduced catalyst increased from 22.4 to 25.0 Å. The reduction of Ni/ZrO_2 increased the nickel metal size more than the carburization after the reaction. The carburized Ni/ZrO_2 catalyst had a catalyst weight gain at 56% but a reduced catalyst at 72%. These results showed that the carburized catalyst exceeded the reduced catalyst and contained less Ni metal.

The changes in the hydrogen formation rate and product selectivity of the Ni/ZrO_2, Ni/V_2O_5 and Ni/Al_2O_3 catalysts versus the reaction temperature are shown in Table 1. At 573 K, the Ni/ZrO_2 exhibited a high formation of hydrogen and CO_2 which gradually increased with the reaction temperature. Methane at 573 K was highly distributed at 57%, but decreased to 9% at 773 K at which the hydrogen formation rate was 1.45 mmol/min/g with 8% CO. The Ni/V_2O_5 catalyst exhibited a low hydrogen formation rate with a high acetaldehyde selectivity and unconverted ethanol at 573 K. At 673 K, the hydrogen formation was increased, while the CO selectivity was decreased. The Ni/V_2O_5 catalyst exhibited a hydrogen formation rate of 1.67 mmol/min/g with 12% CH_4 and 8% CO, and then the highest H_2 rate at the high reaction temperature, although methane was higher than with the Ni/ZrO_2. On the other hand, the ethanol conversion was 100% at 573-773 K for the Ni/Al_2O_3 catalyst. Ethylene and CO were distributed around 60% at 773 K. More ethylene was produced with a lower hydrogen formation as shown in Fig. 1. The ethylene was decomposed to produce carboneous materials, and finally the Ni/Al_2O_3 catalyst was deactivated. CO also produced carbons through the Boudouard reaction ($2CO \rightarrow CO_2 + C$). The BET surface area of the 823 K-carburized 25% Ni/ZrO_2 and 823 K-carburized Ni/V_2O_5 were 12 and 13 m^2/g, respectively. The 25% Ni/Al_2O_3 catalyst had a surface area of 138 m^2/g but was less active for the hydrogen formation selectivity. The Ni/ZrO_2 catalyst exhibited the highest rate of hydrogen formation based on surface area.

In order to determine the difference between the carburization and reduction of the 25% Ni/ZrO_2 catalysts, the SRE on the 823 K-carburized and the reduced Ni/ZrO_2 catalyst at 573 K are shown in Fig. 3. The carburized catalyst continued to have a high activity for 5 h. However, the reduced Ni/ZrO_2 catalyst was less active with large amounts of CO and CH_4 and the activity sharply decreased with the formation of CO and acetaldehyde within 100 min. The reduced catalyst was deactivated. The 823 K-carburized Ni/ZrO_2 catalyst exceeded the 823 K-reduced catalyst and contained Ni carbide and metal and depressed the carbon deposition during the SRE. In a previous paper [27], the zirconia prevented the oxidation of β-Mo_2C at the expense of exchanging ^{18}O of $H_2{}^{18}O$ with $Zr^{16}O_2$ to form $Zr^{16}O_{1-x}{}^{18}O_x$ in combination with doping by the alkali metal, potassium. In this study, zirconia prevented the oxidation of NiC and deactivation.

3.2. Promoting effect of alkali and lanthanide-doped Ni/ZrO_2 on SRE

The promoting effect of the doped-alkali and lanthanide on the activity for the SRE was studied for the development of a highly active Ni/ZrO_2 catalyst. The SRE on the alkali metal-doped $M_{0.01-0.5}Ni_{0.99-0.5}/ZrO_2$ (M = Li, K, Cs) at 773 K is shown in Table 2. The alkali metal doping promoted H_2 formation and CO_2 selectivity and became stable within 7 h. The hydrogen formation increased with a heavier alkali metal (Li < K < Cs), indicating that the alkali metal donated electrons to the nickel and resulted in a more reducing metal [16]. The $K_{0.01}Ni_{0.99}/ZrO_2$ exhibited a value of 1.52 mmol/min g and $Cs_{0.01-0.05}Ni_{0.95-0.99}/ZrO_2$ exhibited a hydrogen formation of 1.53–1.70 mmol/min g. For the $Cs_{0.2}Ni_{0.8}/ZrO_2$ catalyst, the hydrogen formation was the highest at 1.90 mmol/min g and 87% CO_2 selectivity with small amounts of CO and CH_4. The addition of cerium and lanthanum to the Ni/ZrO_2 exhibited hydrogen formation at 1.5 and 1.6 mmol/min g, respectively, showing that the lanthanide addition promoted the hydrogen formation but was less active than the cesium addition.

The Ni/ZrO_2 catalysts with a promoter of Li, K or Ce had a surface area of 10–11 m^2/g, showing no decrease in the surface

Table 1
The hydrogen rate and product selectivity of the catalysts at 573 and 673 K.

Catalyst[a]	Reaction temp. (K)	H_2 formation (mmol/h g)	Area H_2 formation (mmol/h m^2)	Selectivity (%)					
				C_2H_5OH	C_2H_4	CH_3CHO	CH_4	CO	CO_2
Ni/ZrO_2	573	3.49	2.91	–	–	2	57	10.3	30.7
Ni/ZrO_2	673	52.4	5.23	–	–	–	40	2	58
Ni/V_2O_5	573	15.5	1.19	40	–	28.2	24.1	26.5	3.5
Ni/V_2O_5	673	54.0	4.15	0	–	–	39.5	2	56.5
Ni/Al_2O_3	573	25.4	0.18	–	–	3.5	44.5	48	3.8
Ni/Al_2O_3	673	30.0	0.22	–	1	5.5	39	47	9.5

[a] BET surface area of 25% Ni/ZrO_2, 12 (9); 25% Ni/V_2O_5, 13 (9); 25% Ni/Al_2O_3, 138 m^2/g. Bracket was after reaction.

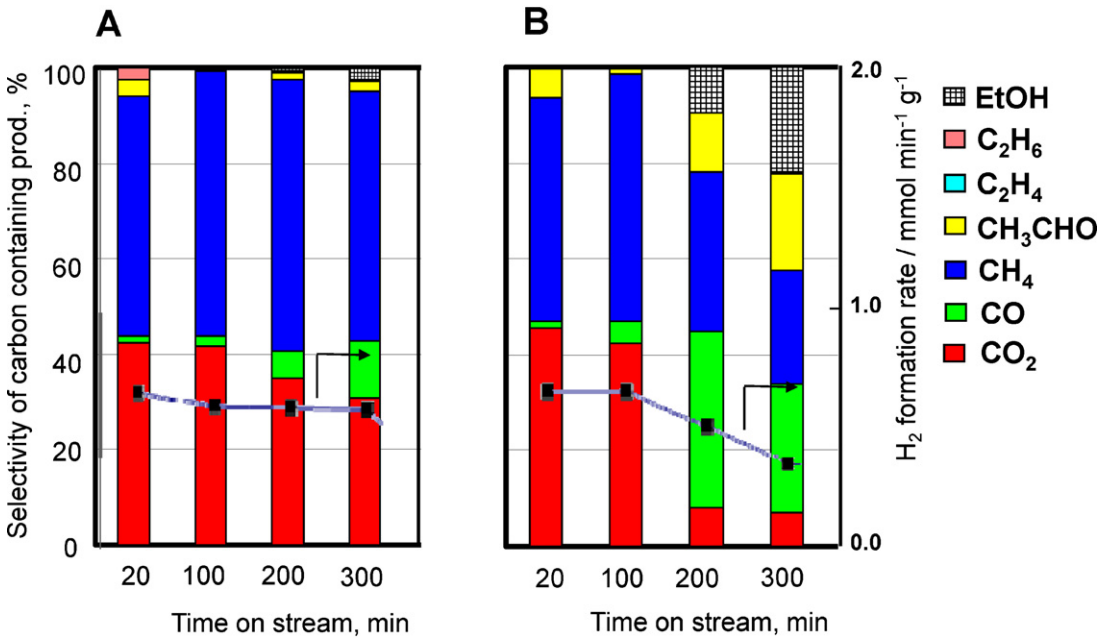

Fig. 3. The hydrogen formation and product selectivity of Ni/ZrO_2 in comparison to (A) the carburization and (B) reduction at 823 K at a reaction temperature of 573 K.

area of zirconia using a doping promoter at 1 mol%. The BET surface areas of $Cs_{0.01}Ni_{0.99}$, $Cs_{0.05}Ni_{0.95}$ and $Cs_{0.2}Ni_{0.8}/ZrO_2$ are 11, 10 and 5 m^2/g, respectively, showing that the Cs addition at less than 5 mol% does not affect the surface area. For the carburized $Cs_{0.2}Ni_{0.8}/ZrO_2$ catalyst, the surface area with micropores decreased to 50–60% compared to the non-doped Ni/ZrO_2 catalyst. Furthermore, the CO adsorption of the carburized Ni/ZrO_2 and $Cs_{0.2}Ni_{0.8}/ZrO_2$ was 47 and 63 μmol/g, respectively, and the sites were 2.4 and 7.8/nm^2. The Cs addition to the Ni/ZrO_2 increased the CO adsorption sites to 325%, although it decreased the surface area to 42%. In a previous paper [22], the irreversible CO adsorption of the 873 K-carburized $Ni_{0.25}Mo_{0.75}$ and $Ni_{0.35}Mo_{0.65}$ was 0.321 and 1.16/nm^2. The 823 K-carburized $Cs_{0.2}Ni_{0.8}/ZrO_2$ had 7.5–4 times the value of the carburized NiMo catalyst due to highly dispersed Ni carbide on the ZrO_2 than the unsupported Ni-Mo bimetallic carbide. As shown in Fig. 4, the 25% $Cs_{0.2}Ni_{0.8}/ZrO_2$ precursor contained NiO (2θ = 37.3, 43.4, and 75.6°; PDF#75-0197), but the carburized $Cs_{0.2}Ni_{0.8}/ZrO_2$ had no NiO (2θ = 37.3°) nor Ni_3C [31,32], but NiC (2θ = 44.4 and 75.4°; PDF#14-0020) and Ni metal (2θ = 44.5 and 76.4°; PDF#87-0712). These peaks proved the formation of Ni carbide from the Ni/ZrO_2 doped with and without Cs. The XRD patterns confirmed the formation of Ni metal and carbide in 20% CH_4/H_2. This XRD result showed that Ni metal was carburized at 656–1000 K for the undoped Ni/ZrO_2. The added cesium oxides were not observed after the carburization at 823 K, although $CsNO_2$ was observed before calcination. The nickel carbide, nickel metal and cesium were dispersed on ZrO_2 for the 823 K-carburized $Cs_{0.2}Ni_{0.8}/ZrO_2$.

3.3. Carbon deposition

The carbon deposition of the various additive-doped Ni/ZrO_2 catalysts after the reaction is shown in Table 3. If the catalyst weight increase in the carburized non-doped Ni/ZrO_2 catalyst was 100%, the Cs-doping at 1 and 5% prevented the carbon deposition by 68 and 45% compared to the non-doped Ni/ZrO_2, respectively. The $Cs_{0.1}Ni_{0.9}/ZrO_2$ and $Cs_{0.2}Ni_{0.8}/ZrO_2$ exhibited no carbon deposition at 7 h. These catalysts effective in anti-carbon-deposition were superior to Rh/MgO and K-Ni/MgO catalyst (1.0 and 2.5 mg carbon/g-cat/h, respectively) [18]. Furthermore, the low

Table 2
SRE on various alkali and lanthanide metals-doped 25% Ni/Zr catalysts carburized at 823 K at the reaction temperature of 773 K for 6.5 h.

Metal-doped Ni/ZrO_2	BET surface area (m^2/g)	H_2 formation (mmol/min g)	Selectivity (%)		
			CH_4	CO	CO_2
Ni/ZrO_2	12	1.45	13	6	81
$Li_{0.01}Ni_{0.99}/ZrO_2$	11	1.45	13	5	82
$K_{0.01}Ni_{0.99}/ZrO_2$	10	1.52	15	4.5	80.5
$Cs_{0.01}Ni_{0.99}/ZrO_2$	11	1.53	14	6	80
$Cs_{0.05}Ni_{0.95}/ZrO_2$	10	1.70	12	6	82
$Cs_{0.1}Ni_{0.9}/ZrO_2$	–	1.73	7	9	84
$Cs_{0.2}Ni_{0.8}/ZrO_2$	5	1.90	6	7	87
$Cs_{0.5}Ni_{0.5}/ZrO_2$	–	1.73	6	7	87
$La_{0.05}Ni_{0.95}$ ZrO_2	–	1.60	6	6	88
$Ce_{0.01}Ni_{0.99}/ZrO_2$	1	1.50	8	7	85

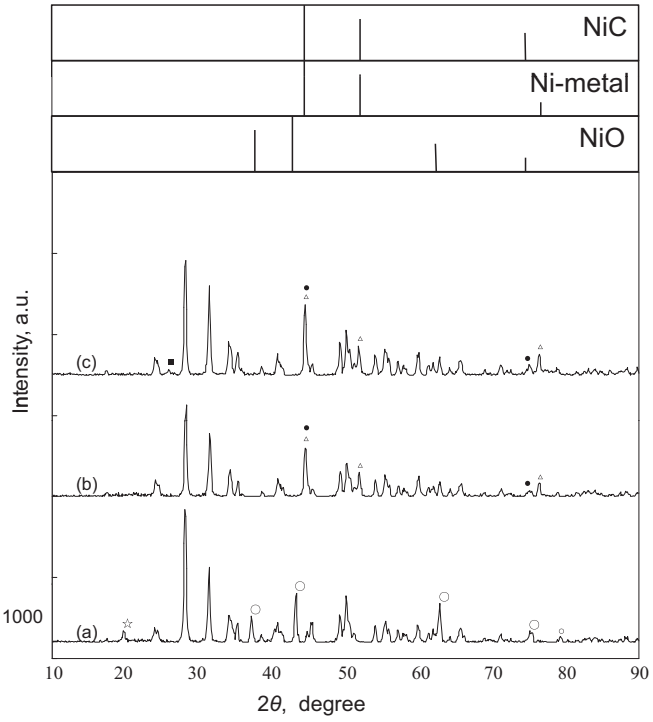

Fig. 4. XRD patterns of (a) 25% $C_{0.2}Ni_{0.8}/ZrO_2$ and 823 K-carburized 25% $C_{0.2}Ni_{0.8}/ZrO_2$ (b) before and (c) after reaction. (•) NiC, (Δ) Ni metal, (○) NiO, (☆) $CsNO_3$ and carbon, while the others are ZrO_2.

concentration of doped metals (K, Li, Ce, and La) at 1–5% prevented the carbon deposition by 75% compared to the non-doped Ni/ZrO_2. The 20% lanthanum addition controlled the carbon deposition better than the cerium addition (a carbon deposition of 66%). Moreover, the reduced $Cs_{0.2}Ni_{0.8}/ZrO_2$ catalyst exhibited a 129% greater carbon deposition than the carburized catalyst. The carburized catalyst prevented carbon deposition better than the reduced catalyst due to the formed Ni carbide during the SRE. Additionally, the cesium addition to the Ni/ZrO_2 catalyst effectively resisted the deposition of graphite carbon and prevented the carbonate and acetate species which were oxidized to produce hydrogen and CO_2. The steam reforming of bioethanol derived from wood was performed for $Cs_{0.2}Ni_{0.8}/ZrO_2$ at 773 K (Table 4).

Table 3
25% Me_xNi_{1-x}/ZrO_2 Catalyst weight gain after SRE at 773 K and at 8 h after run.

Catalyst carburized at 823 K[a]	Catalyst weight increase (%)[b]	Carbon deposit (g)
$25\%Ni/ZrO_2$	100	0.056
$Cs_{0.01}Ni_{0.99}/ZrO_2$	68	0.038
$Cs_{0.05}Ni_{0.95}/ZrO_2$	45	0.025
$Cs_{0.1}Ni_{0.9}/ZrO_2$	0	0
$Cs_{0.2}Ni_{0.8}Ni/ZrO_2$	0 (25)[e]	0 (0.014)[e]
$K_{0.01}Ni_{0.99}/ZrO_2$	80	0.045
$Li_{0.01}Ni_{0.99}/ZrO_2$	98	0.055
$Li_{0.05}Ni_{0.95}/ZrO_2$	89	0.050
$Ce_{0.01}Ni_{0.99}/ZrO_2$	102	0.057
$Ce_{0.05}Ni_{0.95}/ZrO_2$	100	0.056
$Ce_{0.2}Ni_{0.8}/ZrO_2$	66	0.037
$La_{0.05}Ni_{0.95}/ZrO_2$	75	0.042
$La_{0.2}Ni_{0.8}/ZrO_2$	27	0.015
$Cs_{0.2}Ni_{0.8}/ZrO_2$ (bioethanol)[c]	438	0.245
$Cs_{0.2}Ni_{0.8}/ZrO_2$ (reduced)[d]	129	0.072

[a] 0.2 g, carburized at 823 K.
[b] Based on the catalyst weight increase for 25% Ni/ZrO_2 catalyst at post-reaction.
[c] Bioethanol produced from a Japanese cedar.
[d] Reduced at 823 K.
[e] 60 h.

Table 4
The hydrogen formation during the stream reforming of bioethanol and aqueous ethanol solution on the 823 K-carburized 25% $Cs_{0.2}Ni_{0.8}/ZrO_2$ at 773 K.

Reaction time (h)	H_2 formation (mmol/min·g)			
	1	10	30	60
Ethanol/H_2O	2.10	1.90	1.90	1.95
Bioethanol/H_2O	1.65	1.50	1.60	1.60

The hydrogen production was 1.60 mmol/min g over 60 h, and was expected to maintain its durability for a long-time run. The catalyst activity decreased to approximately 84% compared to the feed of an aqueous ethanol solution which had an almost constant activity during the SRE. The carbon deposited was 1.8 times more for the bioethanol feed than that for the feed of an aqueous ethanol solution. This depression was probably due to inhibition by small amounts of lipid, oxygen and sulfur-containing compounds in the bioethanol.

3.4. Temperature-programmed carburization and reduction

The formation of H_2O, CO and CO_2 during the TPC of $Cs_{0.2}Ni_{0.8}/ZrO_2$, Ni/ZrO_2 and Cs/ZrO_2 in a stream of 20% CH_4/H_2 is shown in Fig. 5 to determine the reduction of NiO and Cs_2O and carburization of NiO. A large peak of H_2O was formed by the reduction of NiO in a stream of H_2 and peaks of CO and CO_2 from the decomposition of CH_4 on NiO. Regarding the H_2O formation, $Cs_{0.2}Ni/ZrO_2$ showed two distinct formation temperatures in the region of 519–540 K and 627–656 K and a broad, low peak at 700–870 K. The 25% Ni/ZrO_2 without Cs exhibited one low temperature region of 526–550 K due to the Ni reduction, while the Cs/ZrO_2 exhibited another temperature region of 621–636 K due to the Cs_2O reduction with a small peak at 745 K. The TPR of 25%Ni/ZrO_2 (Fig. 6) in a stream of 100% H_2 showed H_2O peaks at 487, 511 and 537 K together with small shoulder peaks at 573 and 600 K. The H_2O formation peaks during the TPR obviously shifted the temperature peak down by 15 K, compared to that for the TPC peaks in a stream of 20% CH_4/H_2. The reduction with H_2 rapidly formed Ni metal from NiO at 519–540 K. Bellido and Assaf [13] studied the TPR and XRD of Ni supported on ZrO_2, ZrO_2–Y_2O_3 and ZrO_2–CaO and reported that the three TPR peaks corresponded to the reduction of (1) NiO influenced by the oxygen vacancies, (2) NiO in the vicinity of oxygen vacancies, and (3) NiO species that strongly interacted with the support, but not in contact with the oxygen vacancies. Therefore, the peaks at 487 K were due to the reduction of NiO (1), 511 K (2) and 537 K (3) in this study. The low temperature of H_2O desorption was due to the reduction of NiO to Ni metal and a high temperature due to the reduction of Cs_2O below 745 K. H_2O evolution during the TPC for the Ni species of Ni/ZrO_2 and $Cs_{0.8}Ni_{0.5}/ZrO_2$ was observed at less than 690 K. Furthermore, as shown in Fig. 5B, the CO formation was observed at 519–540 and 627–656 K and very small peaks at 870 K coincidental with H_2O formation during the decomposition of 20% CH_4 for $Cs_{0.2}Ni_{0.9}/ZrO_2$, while the Cs-undoped 25% Ni/ZrO_2 had very broad peaks of the CO peak from 656 to 1000 K. These results indicated that the doped Cs assisted the nickel carburization at around 654 K for $Cs_{0.2}Ni_{0.8}/ZrO_2$.

3.5. IR study during temperature-programmed surface reaction after adsorption of ethanol

The infrared spectra for $Cs_{0.2}Ni_{0.8}/ZrO_2$ and Ni/ZrO_2 during the TPD after the ethanol adsorption are shown in Fig. 7. As shown in Fig. 7A, the CH_3 species ($\delta_a(CH_3)$ 1381 and 1454 cm^{-1}; $\nu_a(CH_3)$ 2971 and $\nu_s(CH_3)$ 2864 cm^{-1}) and CH_2 species ($\nu_s(CH_2)$ 2896 cm^{-1}) of the adsorbed ethoxide and bidentate carbonate species ((COO), 1121 and 1061 cm^{-1}) were observed at 373 K for Ni/ZrO_2 [33,34].

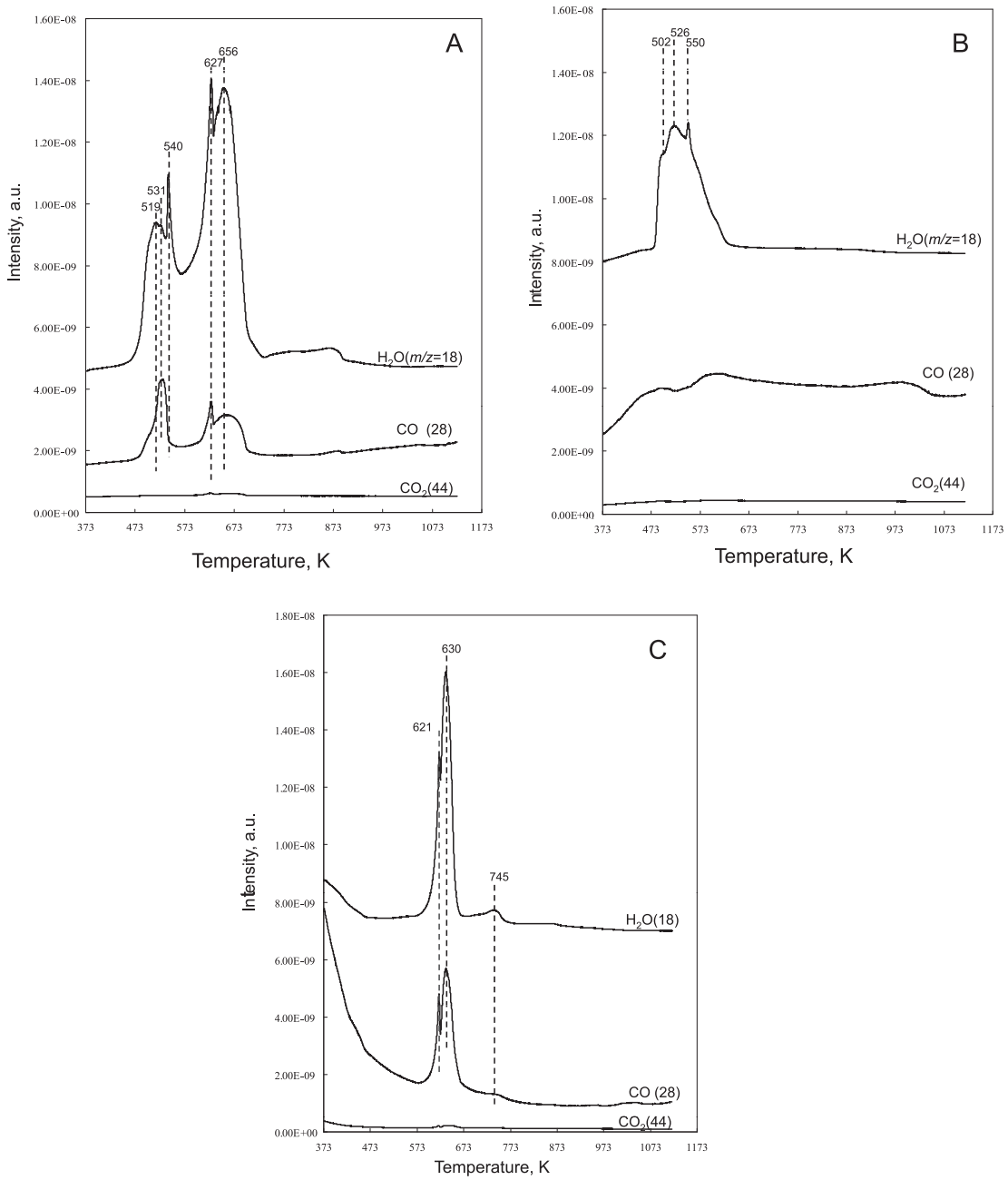

Fig. 5. Desorption of products during the temperature programmed carburization of (A) 25% Cs-doped Ni/ZrO_2, (B) 25% Ni/ZrO_2 and (C) 7% Cs/ZrO_2.

The molecularly adsorbed ethanol was observed due to the bands at 2860–3000 cm^{-1} of δ(OH) (1263 cm^{-1}). These species disappeared at 473 and 573 K, whereas the bands assigned to the acetate species (1559, 1420, 1545 and 1425 cm^{-1} for $Pt/CeZrO_2$ [35]) and (ν(COO), 1549 and 1420 cm^{-1} for Co/ZrO_2 [36]) were observed together with the formation of gaseous CO_2 (2360–2366 cm^{-1}) instead of the adsorbed ethoxide species. The carbonate bands ((CO_3) 1549, 1420, 1263 and 1018 cm^{-1} (1549, 1131 and 1018 cm^{-1})) attributed to the formed CO_2 were observed as reported before [37], which suggested $CO_2 + O_2^- \rightarrow CO_3^-$. The carbonate and acetate species were extensively adsorbed based on the IR spectra, but acetaldehyde and acetic acid were not formed during the steam reforming of these species. On the other hand, the Cs-doped Ni/ZrO_2 had spectra different from those of Ni/ZrO_2 in Fig. 7B. Bands were observed at 1645 cm^{-1} and 373 K and large bands at 1616 and 1308 cm^{-1} together with those around 1534, 1412 and 1392 cm^{-1}. The bands at 1645 and 1305 cm^{-1} were due to the acetate and carboxylic species by the adsorption of acetic acid at 373 K. The CH_2 species (2896 cm^{-1}, CH_3 (1457) and CH_3 (2864 cm^{-1}) of the adsorbed ethoxide and the bidentate species (1117 and 1056 cm^{-1}) were observed at 373 K. Above 473 K, the band at 1616 cm^{-1} was possibly due to H_2O formation with the corresponding broad H_2O bands at 3500–4000 cm^{-1}. The hydrogen carbonate species (I) (ν(CO_3), 1616, 1412, and 1108 cm^{-1} and (II) (ν(CO_3), 1616 and 1392 cm^{-1} [38]) and CO (ν(CO), 2200 and 2188 cm^{-1} at 573 K) were observed along with gaseous CO_2 (2365–2342 cm^{-1}). Gaseous CO_2 was adsorbed and CO_2 vigorously reacted with the surface O_2^- to form hydrogen carbonate and bidentate carbonate species but strongly adsorbed on ZrO_2 of the Ni/ZrO_2 catalyst. These formed species were not desorbed into the gas phase. The small band at

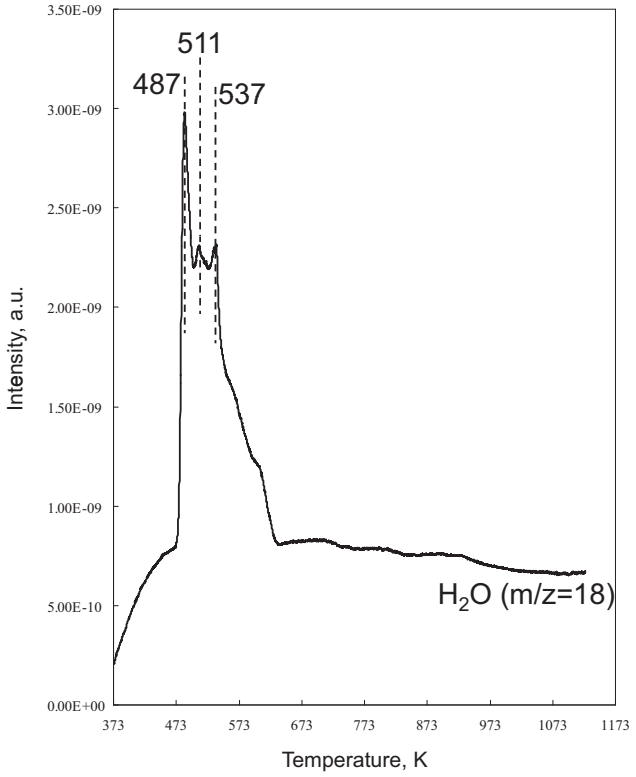

Fig. 6. The desorption of H_2O during the temperature programmed reduction of 25% Ni/ZrO_2.

1728 cm^{-1} above 473 K was probably assigned to C=O stretches in the acetyl species (CH_3CO) [33,36,39,40].

3.6. Reaction scheme for SRE on $CsNi/ZrO_2$ based on TPD after the adsorption of ethanol

The TPD of the 823 K-carburized $Cs_{0.2}Ni_{0.8}/ZrO_2$, Ni/ZrO_2 and ZrO_2 after ethanol adsorption is shown in Fig. 8. The SRE reaction mechanism on the 823 K-carburized Cs-doped Ni/ZrO_2 catalyst is shown in Fig. 9. The TPDs of ethanol are discussed using the step number in the reaction mechanism of SRE. For the TPD of Ni/ZrO_2 (Fig. 8A) after ethanol adsorption, the evolution of gases was observed in two temperature regions. A sharp peak of hydrogen was observed at 489 K together with CH_4 and CO at 496–511 K. Ethanol was adsorbed on the ethoxide species (step 1), and subsequently formed the CH_3CHO species with H_2 evolved (step 2). CO_2 was detected together with H_2O, CH_4 and CO at the peaks of 503–511 K. Methane and CO were formed through the CH_3CHO species. $CH_3CHO_{(a)} \rightarrow CH_{3(a)} + CO_{(a)}$. $CH_{3(a)} + H_{(a)} \rightarrow CH_4$ (step 8), where (a) stands for adsorbed. $CO_{(a)} \rightarrow CO_{(g)}$ or $CO_{(a)} \rightarrow C_{(a)} + O_{(a)}$ (step 9). These species are the same ones formed from step (5). As a result, carbon dioxide and water were formed in steps 6 and 7. On the other hand, for the $Cs_{0.2}Ni_{0.8}/ZrO_2$ catalyst (Fig. 8B), hydrogen and H_2O were formed along with a small amount of CO_2 at the peak of 406–430 K. No release of CH_4, CO, ethylene and CH_3CHO occurred. H_2O, CH_4, CO and CO_2 were formed at the peak of 565 K without hydrogen as well as the H_2O and CO_2 at 602 and 630 K for $Cs_{0.2}Ni_{0.8}/ZrO_2$. The Cs-doped Ni/ZrO_2 catalyst promoted the formation of $CH_3CO_{(a)}$ at 1728 cm^{-1} (step 3), along with successive C–H bond breaking (step 4) and leading to C–C bond breaking to $[C \text{ and } O]_{(a)}$ (step 5) and finally producing CO_2 and H_2O (steps 6 and 7). No methane formation showed no methanation ($CO + 3H_2 \rightarrow CH_4 + H_2O$) through $CO_{(a)}$ formed from in steps 6 and 8. Second peaks at around 600 K for the strongly adsorbed CH_3CHO and CH_3COO which were decomposed to H_2, H_2O and CO_2. Based on the results, NiC, Ni metal and cesium covered the ZrO_2 surface, and the Cs addition promoted H_2 formation with less formation of CH_4 and CO. The adsorbed CH_3CO was formed in step 3 and converted to $C_{(a)}$ and $O_{(a)}$ (step 5). The $CH_3CO_{(a)}$ would not be converted to CH_4 and CO (step 8; C–C bond breaking) nor $C_2H_5OH_{(a)}$ to C_2H_4 using ZrO_2 and Ni/Al_2O_3 [12,14,15], but the successive C–H bond breaking to $[C \text{ and } O]_{(a)}$ species on the carburized $Cs_{0.2}Ni_{0.8}/ZrO_2$ was observed. Consequently, $Cs_{0.2}Ni_{0.8}/ZrO_2$ helped to facilitate the dissociation of H_2O to 2H and O as well as the dehydrogenation of CH_3CO to CHCO species, leading to $[C \text{ and } O]_{(a)}$. This mechanism of acetyl formation and the decomposition to CO_2 and H_2O was reported by Nagai and Gonzalez obtained from the oxidation of ethanol and acetaldehyde on $1\%Pt/SiO_2$ catalyst [39]. This acetyl is a key reaction intermediate dissociated to co-adsorbed CO and CH species with almost no barrier on ethanol synthesis from syngas [41]. Thus, the Cs-activated Ni carbide likely facilitated the hydrogen and CO_2 formation from ethanol through the CH_3CO species. For ZrO_2 alone (Fig. 8C), hydrogen, CO and ethylene were observed at 590 K, desorbing ethanol and acetaldehyde at low temperature. Ethylene was desorbed from dehydration of $CH_5OH_{(a)}$ on the acidic sites of ZrO_2. The remaining adsorbed CH_3CHO was decomposed and desorbed as hydrogen, CO and CO_2 at 770 K.

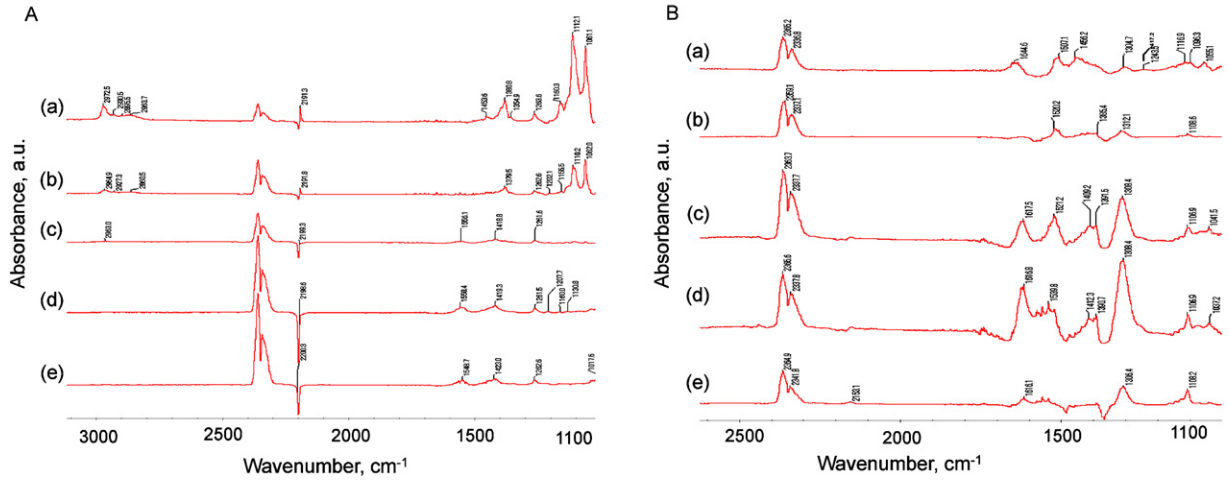

Fig. 7. IR spectra of the 823 K-carburized (A) 25% Ni/ZrO_2 and (B) 25% $Cs_{0.2}Ni/ZrO_2$ catalysts at (a) 373, (b) 423, (c) 473, (d) 523 and (e) 573 K during TPD.

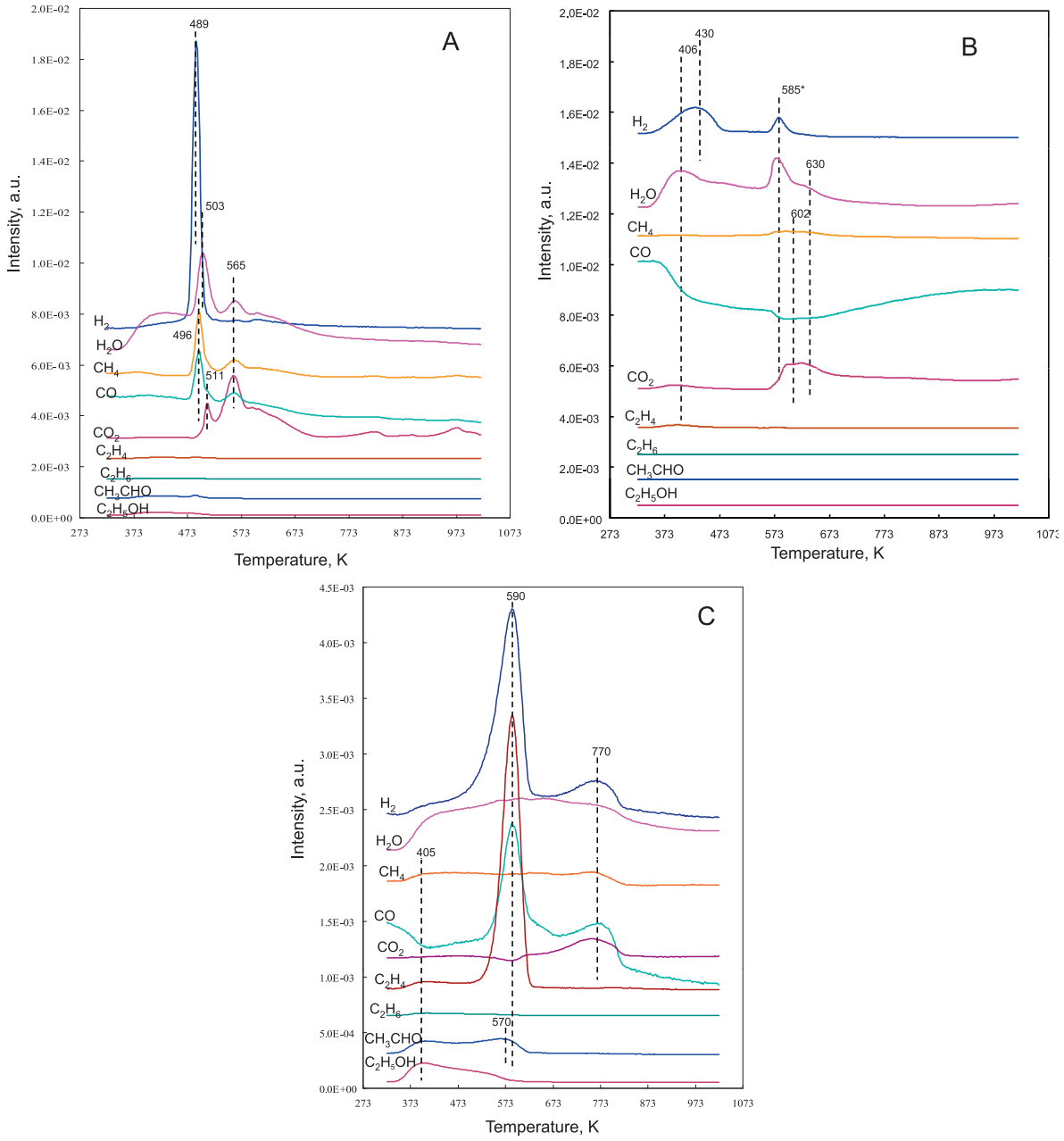

Fig. 8. MS profiles during the temperature-programmed desorption of (A) 25% Ni/ZrO_2, (B) 25% $Cs_{0.2}$-doped $Ni_{0.8}/ZrO_2$ and (C) ZrO_2 catalyst after ethanol adsorption.

The TPD for the $Cs_{0.2}Ni_{0.8}/ZrO_2$ catalyst was performed after the adsorption of C_2H_5OD instead of C_2H_5OH (Fig. 10) in order to confirm the contribution of the dissociated H and remaining CH_3CHO to the formation of hydrogen, water and CO_2. The *m/z* values of 3 and 19 were observed for the HD and HOD formation on $Cs_{0.2}Ni_{0.8}/ZrO_2$, respectively, with a large amount of hydrogen and H_2O (steps 1–4, 10: hydrogen formation from C–H bond breaking). $D_2{}^{16}O$ was hardly observed during the TPD of C_2H_5OD. For $Cs_{0.2}Ni_{0.8}/ZrO_2$ catalyst, the adsorbed ^{16}O was reacted with D from C_2H_5OD or H from water to form $HD^{16}O$ in step 7. Also, the $D_{(a)}$ and $H_{(a)}$ reacted with each other to form $HD_{(a)}$ as well as $2H_{(a)}$ (step 11). Regarding methane formation, *m/z* = 16 was observed and but *m/z* = 15 was not desorbed as a second fragmentation peak of CH_4. In addition, the *m/z* = 17 (CH_3D) was observed, but acted as *m/z* = 18 and 19 (water). Therefore, *m/z* = 17, 18 and 19 were due to the fragmentation of H_2O. This result showed no formation of methane (step 8) during the TPD of $Cs_{0.2}Ni_{0.8}/ZrO_2$ as well as no hydrogenation of the $CO_{(a)}$ formed in step 6. Moreover, CO_2 and CH_3CHO might be observed as (*m/z* = 44) at 575 and 602 K. CO_2 has a strong intensity of *m/z* = 44 (M^+), while acetaldehyde has MS fragments of *m/z* = 15, 19 (M^+), 43 and 44. No strong peak of *m/z* = 19 was observed, and therefore, *m/z* = 44 was a molecular ion peak of CO_2. A pulse injection of $H_2{}^{18}O$ into the C_2H_5OH stream during the SRE on $Cs_{0.2}Ni_{0.8}/ZrO_2$ was performed at 773 K. As shown in Fig. 11, $C^{18}O$, $C^{18}O_2$ and $C^{16}O^{18}O$ were formed together with small amounts of $C^{16}O$ and $C^{16}O_2$. The water was dissociated into hydrogen and oxygen. Step 10 contains: $H_2{}^{18}O_{(a)} \rightarrow {}^{18}OH_{(a)} + H_{(a)} \rightarrow {}^{18}O_{(a)} + 2H_{(a)}$. A 973 K-carburized 4.8 and 8.5% Mo/Al_2O_3 catalysts facilitated the dissociation of CO and H_2O as well as the dissociation-association mechanism ($^{13}C^{16}O \rightarrow {}^{13}C + {}^{16}O$, $^{13}C^{16}O + {}^{16}O \rightarrow {}^{13}C^{16}O_2$) [42]. Potassiium- and zirconium-promoted cobalt molybdenum carbide is also reported to undergo water and CO dissociation [27]. The adsorbed CH_3CO formed in step 3 and was converted to $C_{(a)}$ and $O_{(a)}$ (step 5). $C_{(a)} + {}^{18}O_{(a)} \rightarrow C^{18}O_{(a)}$. $C^{18}O_{(a)} + {}^{18}O_{(a)} \rightarrow C^{18}O_{2(a)}$.

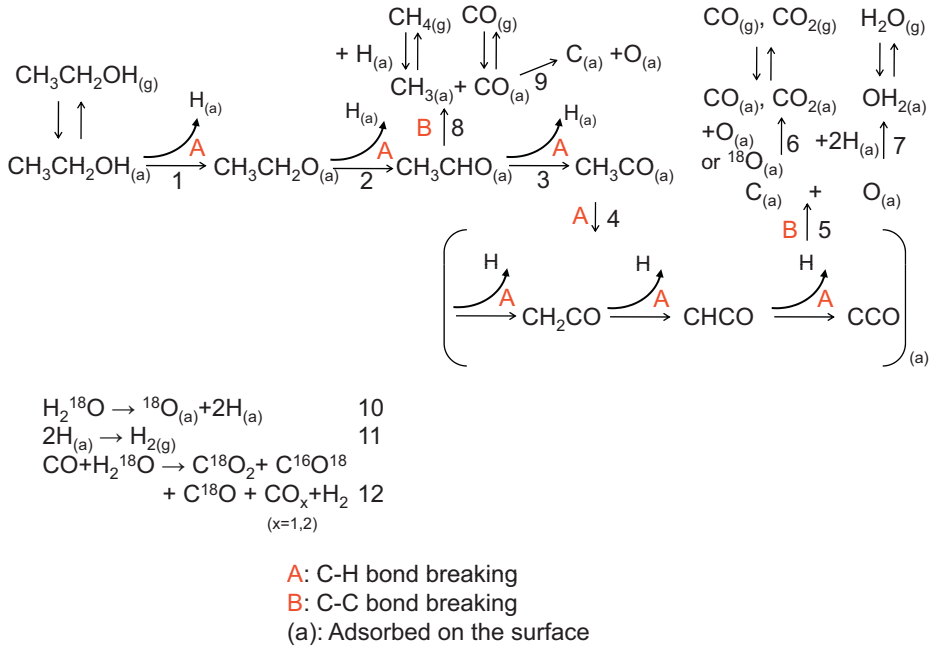

Fig. 9. Scheme of steam reforming of ethanol on $CsNi/ZrO_2$.

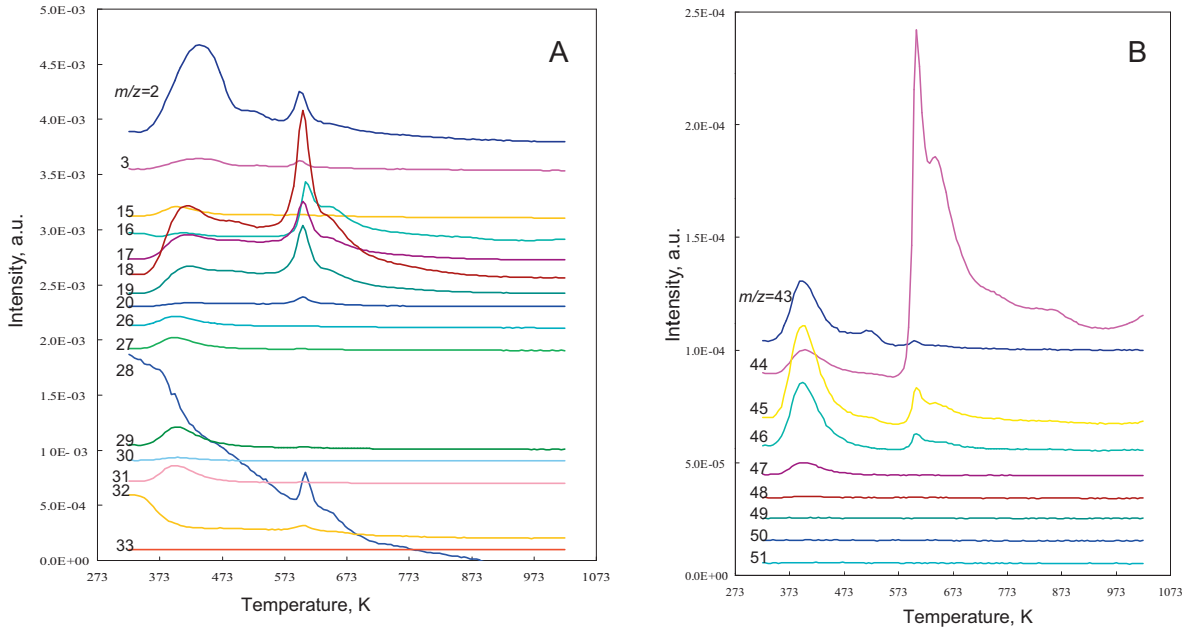

Fig. 10. MS profiles (A: m/z = 1–42 and B:43–51) during the temperature-programmed desorption of the 25% $Cs_{0.2}Ni_{0.8}/ZrO_2$ catalyst after C_2H_5OD adsorption.

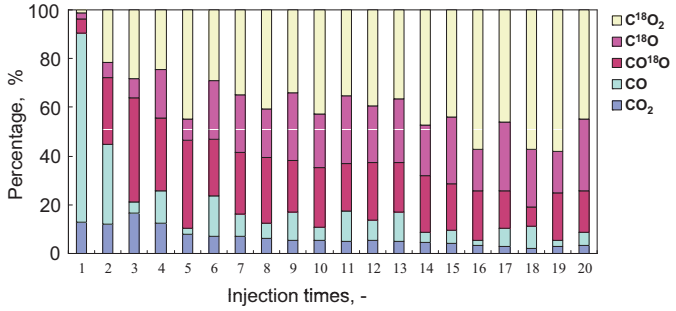

Fig. 11. The change in the reaction products of carbon dioxide and carbon monoxide in the pulse of $H^{18}O$ into the SRE on the $Cs_{0.2}Ni_{0.8}/ZrO_2$ catalyst.

These steps were the main formation of carbon dioxide. $C^{16}O_{(a)} + {}^{18}O_{(a)} \rightarrow C^{16}O^{18}O_{(a)}$. In addition, the water–gas shift reaction showed $CO + H_2{}^{18}O \rightarrow C^{16}O^{18}O_{(a)} + 2H_{(a)}$. Thus, the Cs-doped Ni/ZrO_2 catalyst is useful for the steam reforming of ethanol (ethanol: water = 1:13) at 773 K to produce hydrogen at 1.95 mmol/min/g-cat during 60 h.

4. Conclusions

The effects of several supports such as ZrO_2, V_2O_5, CeO_2, MgO and Al_2O_3 on the activities and the properties of the Ni carbide catalysts were studied for the reaction conditions of 573–773 K, a N_2 gas flow of 0.9 L/h, an aqueous solution of ethanol (C_2H_5OH:H_2O

molar ratio 1:13) and a flow rate of 12 mL/h. The $Cs_{0.2}Ni_{0.8}/Zr$ catalyst exhibited hydrogen formation of 1.9 mmol/min g and 82% CO_2 selectivity with trace amounts of CO and CH_4, which was more active than was the addition of Li, K, Ce and La to the Ni/ZrO_2. The TPO result of $Cs_{0.2}Ni_{0.8}/ZrO_2$ and spent Ni/ZrO_2 showed that the CO_2 evolutions are due to the oxidation of the carbonate and acetate species, pyrolytic carbon, Ni carbide and graphite carbon. The $Cs_{0.2}Ni/ZrO_2$ and $Cs_{0.5}Ni_{0.5}/Zr$ exhibited no carbon deposition at 7 h. The carburization and cesium-doped Ni/ZrO_2 were more effective in decreasing the carbon deposition. From the IR study, the formed carbonated species were attributed to the formation of CO_3^- from the formed CO_2 ($CO_2 + O_2^- \rightarrow CO_3^-$). In the pulse experiment of $H_2{}^{18}O$, the ethanol stream during the SRE on $Cs_{0.2}Ni/ZrO_2$ at 773 K, $C^{18}O_2$, $C^{18}O$ and $C^{18}O^{16}O$ were formed together with trace amounts of ^{16}CO and $^{16}CO_2$. This result showed that $Cs_{0.2}Ni/ZrO_2$ helped to facilitate the dissociation of H_2O to 2H and O and the decomposition of CH_3CHO to hydrogen and CO_2 through the CH_3CO species. The TPD after ethanol adsorption on Ni/ZrO_2 with and without Cs-doping showed that the $Cs_{0.2}Ni_{0.8}/ZrO_2$ catalyst promoted the C–H breaking through the CH_3CO species more than did the Ni/ZrO_2 catalyst.

References

[1] J. Kugai, S. Velu, C. Song, M.H. Engelhard, Y.-H. Chin, J. Catal. 238 (2006) 430.
[2] J.P. Breen, R. Burch, H.M. Coleman, Appl. Catal. B: Environ. 39 (2002) 65.
[3] G.A. Deluga, J.R. Salge, L.D. Schmidt, X.E. Verykios, Science 303 (2004) 993.
[4] W. Cai, F. Wang, E. Zhan, A.C. Van Veen, C. Mirodatos, W. Shen, J. Catal. 257 (2008) 96.
[5] H. Song, U.S. Ozkan, J. Catal. 261 (2009) 66.
[6] S.S.-Y. Lin, D.H. Kim, M.H. Engelhard, S.Y. Ha, J. Catal. 273 (2010) 229.
[7] J. Lorca, J.-A. Dalmon, P.R. de la Piscina, N. Homs, Appl. Catal. A: Gen. 243 (2003) 261.
[8] B. Zhang, X. Tang, Y. Li, W. Cai, Y. Xu, W. Shen, Catal. Commun. 7 (2006) 367.
[9] A.N. Fatsikostas, D.I. Kondarides, X.E. Verykios, Catal. Today 75 (2002) 145.
[10] J. Sun, X.-P. Qiu, F. Wu, W.-T. Zhu, Int. J. Hydrogen Energy 30 (2005) 437.
[11] T. Miyazawa, T. Kimura, J. Nishikawa, S. Kado, K. Kunimori, K. Tomishige, Catal. Today 115 (2006) 254.
[12] N. Laosiripojana, S. Assabumrungrat, S. Charojrochkul, Appl. Catal. A: Gen. 327 (2007) 180.
[13] J.D.A. Bellido, E.M. Assaf, J. Power Sources 177 (2008) 24.
[14] A.N. Fatsikostas, X.E. Verykios, J. Catal. 225 (2004) 439.
[15] M.C. Sánchez-Sánchez, R.M. Navarro, J.L.G. Fierro, Catal. Today 129 (2007) 336.
[16] J. Juan-Juan, M.C. Román-Martínez, M.J. Illán-Gómez, Appl. Catal. A: Gen. 264 (2004) 169.
[17] F. Frusteri, S. Freni, V. Chiodo, L. Spadaro, O. Di Blasi, G. Bonura, S. Cavallaro, Appl. Catal. A: Gen. 270 (2004) 1.
[18] F. Frusteri, S. Freni, J. Power Sources 173 (2007) 200.
[19] A.E. Galetti, M.F. Gomez, L.A. Arrúa, M.C. Abello, Appl. Catal. A: Gen. 348 (2008) 94.
[20] F. Mariño, G. Baronetti, M. Jobbagy, M. Labored, Appl. Catal. A: Gen. 238 (2003) 41.
[21] A.J. Vizcaíno, A. Carrero, J.A. Calles, Int. J. Hydrogen Energy 32 (2007) 1450.
[22] M. Nagai, A.M. Zahidul, K. Matsuda, Appl. Catal. A: Gen. 313 (2006) 137.
[23] R. Barthos, A. Széchenyi, Á. Koós, F. Solymosi, Appl. Catal. A: Gen. 327 (2007) 95.
[24] A. Széchenyi, F. Solymosi, J. Phys. Chem. C 111 (2007) 9509.
[25] R. Barthos, A. Széchenyi, F. Solymosi, Catal. Lett. 120 (2008) 161.
[26] Y. Miyamoto, M. Akiyama, M. Nagai, Catal. Today 146 (2009) 87.
[27] M. Nagai, A.M. Zahidul, Y. Kunisaki, Y. Aoki, Appl. Catal. A: Gen. 383 (2010) 58.
[28] A.L. Alberton, M.M.V.M. Souza, M. Schmal, Catal. Today 123 (2007) 257.
[29] H.V. Fajardo, L.F.D. Probst, Appl. Catal. A: Gen. 306 (2006) 134.
[30] A.J.W.C. Liberatori, R.U. Ribeiro, D. Zanchet, F.B. Noronha, J.M.C. Bueno, Appl. Catal. A: Gen. 327 (2007) 197.
[31] Y. Leng, L. Xie, F. Liao, J. Zheng, X. Li, Thermochim. Acta 473 (2008) 14.
[32] Y. Goto, K. Taniguchi, T. Omata, S. Otuka-Yao-Matsuo, N. Ohashi, S. Ueda, H. Yoshikawa, Y. Yamashita, H. Oohashi, K. Kobayashi, Chem. Mater. 20 (2008) 4156.
[33] O. Kresnawahjuesa, R.J. Gorte, D. White, J. Mol. Catal. A: Chem. 208 (2004) 175.
[34] J. Raskó, M. Dömök, K. Baán, A. Erdőhelyi, Appl. Catal. A: Gen. 299 (2006) 202.
[35] S.M. de Lima, I.O. da Cruz, G. Jacobs, B.H. Davis, L.V. Mattos, F.B. Noronha, J. Catal. 257 (2008) 356.
[36] J. Llorca, N. Homs, P.R. de la Piscina, J. Catal. 227 (2004) 556.
[37] H. Tominaga, M. Nagai, Appl. Catal. A: Gen. 282 (2005) 5.
[38] C. Binet, M. Daturi, J.-C. Lavalley, Catal. Today 50 (1999) 207.
[39] M. Nagai, R.D. Gonzalez, Ind. Eng. Chem. Prod. Res. Dev 24 (1985) 525.
[40] P. Cheung, A. Bhan, G.J. Suenley, D.J. Law, E. Iglesia, J. Catal. 245 (2007) 110.
[41] D. Mei, R. Rousseau, S.M. Kathmann, V.-A. Glezakou, M.H. Engelhard, W. Jiang, C. Wang, M.A. Gerber, J.F. White, D.J. Stevens, J. Catal. 271 (2010) 325.
[42] T. Namiki, S. Yamashita, H. Tominaga, M. Nagai, Appl. Catal. A: Gen. 398 (2011) 155.